S. D. Guest

S. Pellegrino

Engineering Department,
Cambridge University,
Trumpington Street,
Cambridge, CB2 1PZ U.K.

The Folding of Triangulated Cylinders, Part III: Experiments

This paper describes an experimental investigation of a type of foldable cylindrical structure, first presented in two earlier papers. Three cylinders of this type were designed and manufactured, and were then tested to find the force required to fold them. The results from these tests show some discrepancies with an earlier computational simulation, which was based on a pin-jointed truss model of the cylinders. Possible explanations for these discrepancies are explored, and are then verified by new simulations using computational models that include the effect of hinge stiffness, and the effect of geometric imperfections.

1 Introduction

Foldable structures are used for a variety of applications, ranging from umbrellas to solar arrays for spacecraft. This paper describes an experimental investigation of a type of foldable cylindrical structure, first presented in two earlier papers (Guest and Pellegrino, 1994a, b). These structures are formed by dividing up the surface of a cylinder into a series of identical triangles, the sides of which approximate to helices. The side-lengths of the triangles are chosen such that (i) the cylinder is bi-stable, having two strain-free configurations, one extended and one folded; (ii) the strains induced by the folding process are sufficiently small that the cylinder deforms purely elastically.

The first paper in this series (Guest and Pellegrino, 1994a), henceforth referred to as Part I, introduced this type of foldable cylinders, and described the four topological and geometric parameters that are required to identify a particular cylinder. The parameters are the number of starts of two of the helices on the surface of the cylinders, denoted by the letters a and b, and the ratios between the lengths of two sides of a triangle and the third. With the symbols introduced in Figs. 2 and 3 of Part I, the four parameters are m, n, l_b/l_a, and l_c/l_a, respectively. By considering a simplified, uniform folding mode, Part 1 obtained estimates of the strains induced by folding cylinders with $m = 1$, $n = 7$, and $m = 2$, $n = 7$, for a wide range of ratios l_b/l_a and l_c/l_a.

The second paper in this series (Guest and Pellegrino, 1994b), henceforth referred to as Part II, looked in more detail at the folding process of three particular cylinders, and described a computer simulation of that process. The simulation showed that the folding process is broadly similar in the three cylinders and consists of two distinct phases. During the first phase, the cylinder forms a strained shape-transition region under a steadily increasing folding force. When this force reaches a peak and starts to decrease, the second phase begins. Now, the shape transition region moves along the cylinder under a small force, leaving behind a fully folded part of the cylinder. This type of behavior is observed in the collapse of many structures, and is generally known as a *propagating instability* (Kyriakides, 1994). However, while propagating instabilities are usually destructive, for these cylinders this behavior is highly desirable.

This paper describes three foldable cylinders that have been designed, manufactured, and tested. The first two cylinders were designed simply to validate the theoretical work in the previous papers. The third cylinder was aimed at a possible application, to produce a collapsible fuel tank for Hydrazine, a highly corrosive rocket fuel. As fuel is used, the tank would reduce its volume, thus preventing sloshing of the remaining fuel, and also reducing the amount of fuel which collects away from the supply pipe, and hence is left unused. A summary of the geometry of the cylinders that were manufactured is given in Table 1. The observed experimental behavior shows complexities that were not predicted in Part II. However, a re-analysis of the folding process which allows for two effects that had been neglected previously, hinge stiffness along the connections between panels, and the presence of manufacturing imperfections, predicts the kind of behavior that is observed in practice.

The layout of the paper is as follows. Section 2 describes the manufacture and compression testing of the models, and identifies the key discrepancies between the behavior predicted by the computer simulations in Part II and the actual behavior of the models. Possible explanations for these discrepancies are discussed in Section 3, and these explanations are investigated in detail, in Section 4, by modifying the computer model and producing new simulations. Section 5 discusses these simulations, and concludes the paper.

2 Experiments

Irathane and Aluminium-Alloy Cylinders. Two of the cylinders described in Part I have been made from sheets of 0.9 mm thick aluminium alloy plate, coated with a 0.7 mm thick layer of Irathane on both sides (Irathane is a flexible polyurethane). Hinges were made by forming a series of straight, parallel grooves, using a milling machine. Both one layer of the Irathane and the Al-alloy were removed, thus leaving only one layer of Irathane to form the hinge. Each sheet was milled to the correct fold pattern. The final cylinders were formed by joining together opposite edges of the sheets with small plates. The bases of both cylinders were fully restrained before testing.

Each cylinder was tested using a Howden testing machine in a displacement controlled mode. The top of the cylinder was loaded using a plate attached to the testing machine through a central ball joint, thus allowing the plate to change its orientation during folding. The total compressive load on the cylinder was obtained by adding the weight of the loading plate to the force measured by a load cell, at the top of the testing machine. Once the cylinder had been fully compressed the test was reversed, as further compression would have damaged the connection between the cylinder and the base plate.

The results of the compression test on cylinder no. 1 are shown in Fig. 1(a). This plot of force during folding shows a clear periodicity, where the period is approximately 20 mm.

Contributed by the Applied Mechanics Division of THE AMERICAN SOCIETY OF MECHANICAL ENGINEERS for publication in the ASME JOURNAL OF APPLIED MECHANICS.

Discussion on this paper should be addressed to the Technical Editor, Professor Lewis T. Wheeler, Department of Mechanical Engineering, University of Houston, Houston, TX 77204-4792, and will be accepted until four months after final publication of the paper itself in the ASME JOURNAL OF APPLIED MECHANICS.

Manuscript received by the ASME Applied Mechanics Division, Aug. 1, 1994; final revision, Dec. 23, 1994. Associate Technical Editor: S. Kyriakides.

Table 1 Geometric parameters

	m	n	l_a (mm)	l_b (mm)	l_c (mm)
Irathane and Al-alloy cylinder no. 1	1	8	50.0	50.0	90.1
Irathane and Al-alloy cylinder no. 2	1	7	50.0	50.0	86.6
Cu-Be and steel cylinder	1	7	124.8	104.7	205.3

For this cylinder, the change in the relative height coordinates of two nodes on the a-helix is 2.7 mm between the extended and folded configuration, while this difference is 22 mm for two nodes on the b-helix. Hence, it can be concluded that the basic periodicity of the force plot has a wavelength corresponding to the relative height of successive nodes on the b-helix.

The cylinder formed one transition zone at the top of the cylinder, which moved down the cylinder as the test proceeded. As displacement δ was increased, no triangles would fold while the force was increasing, but several triangles folded in quick succession while the force was decreasing.

The results of the compression test on cylinder no. 2 are shown in Fig. 1(b). For this case the change in the relative height coordinates of two successive nodes between the extended and folded configuration is 4.0 mm along the a-helix, and 28 mm on the b-helix. The behavior of cylinder no. 2 was similar to the previous cylinder, except that in this case there is no consistent periodicity in the results.

Cu-Be and Steel Cylinder. The third cylinder was manufactured using a copper beryllium alloy (Cu-Be) as a hinge material. Cu-Be was used because, when correctly heat-treated, it has a large elastic strain range and hence a thin strip of Cu-Be can be elastically bent around a small radius. The cylinder was made from a flat, 0.1 mm thick sheet of Cu-Be. A series of stiff triangular panels were formed by sandwiching the Cu-Be between triangles of 0.5 mm thick steel plate. These plates were spot welded in place. Then, the two edges of the sheet were joined together, to form the cylinder. Note that steel plates could not be used for a Hydrazine tank, as the steel and the Hydrazine would react. A different stiffening material would have to be used.

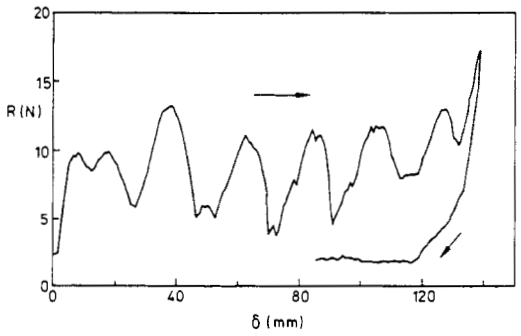

Fig. 1(a)

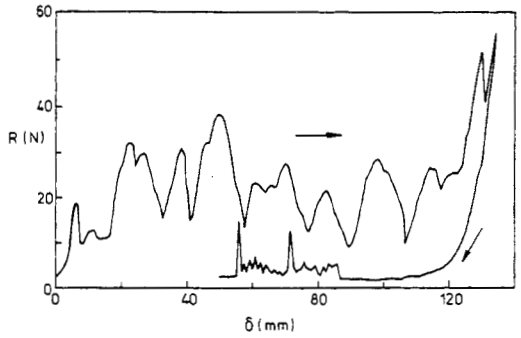

Fig. 1(b)

Fig. 1 Force required to compress the Irathane and Al-alloy cylinders: (a) Cylinder no. 1, (b) Cylinder no. 2

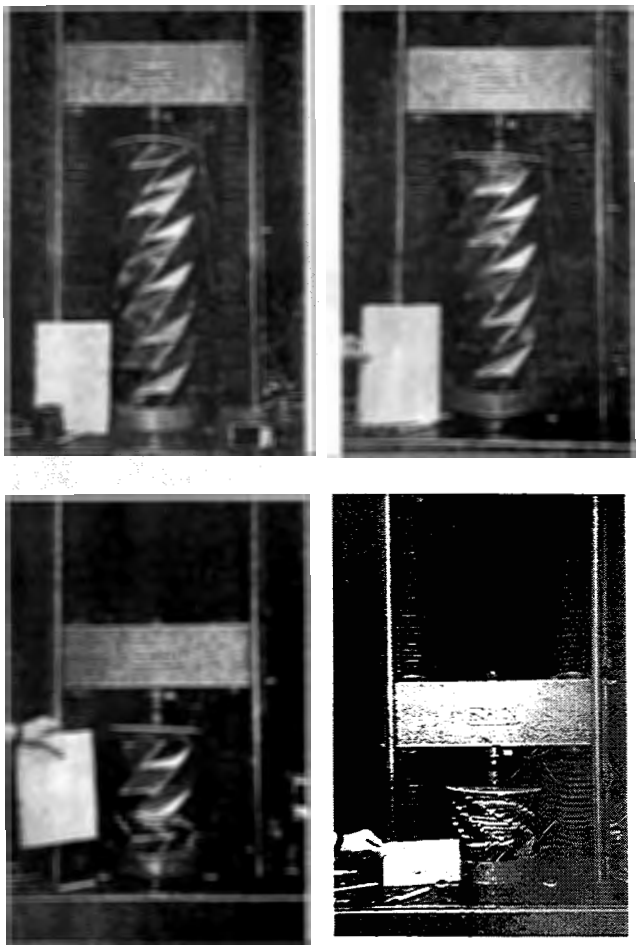

Fig. 2 Folding of the Cu-Be and steel cylinder: initial state, δ = 100 mm; δ = 400 mm; δ = 630 mm, fully folded

The steel triangles were placed 6 mm apart on the Cu-Be sheet to allow an elastic hinge to form. Also, the corners of the steel plates were rounded, to increase the width of the unrestrained Cu-Be sheet near the intersection of hinge lines. One problem with this method of construction is the detail of folds around a node. Inevitably there is an incompatibility where concave and convex folds meet. At this point a crease forms in the Cu-Be sheet, causing plastic deformation. Thus the aim of purely elastic folding was not entirely achieved in this design. The base of the cylinder was fully fixed, by casting it into an epoxy base.

Four compression tests were performed, following the same procedure as for the Irathane and Al-alloy cylinders. Figure 2 shows four photographs taken during the first test. It can be seen from the first photograph that the cylinder had to be initially slightly folded to fit in the testing machine. A plot of the force required to fold the cylinder during this test, Fig. 3(a), shows a period of approximately 60 mm. The change in relative height coordinates of two successive nodes between the extended and the folded configuration is 9 mm along the a-helix, and 64 mm along the b-helix, and so clearly the periodicity of the plot corresponds to the folding of successive nodes on the b-helix.

One important effect shown in Fig. 2 is the formation of a second transition zone close to the base of the cylinder. This

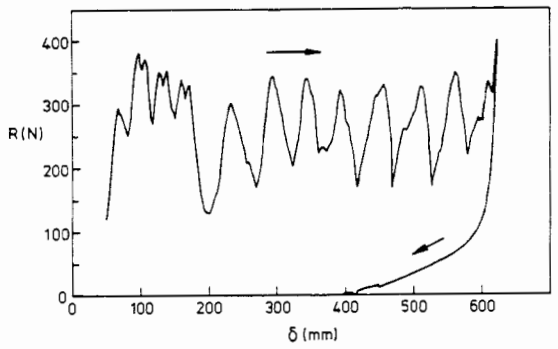

Fig. 3(*a*)

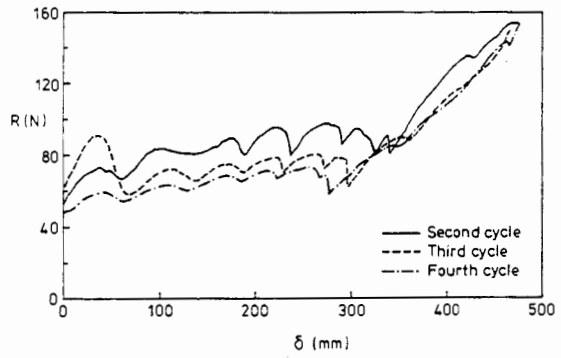

Fig. 3(*b*)

Fig. 3 Force required to compress the Cu-Be and steel cylinder: (*a*) first test, (*b*) second, third, and fourth tests

occurred when the cylinder had been compressed by 125 mm. For the rest of the test it was this transition zone which moved up through the cylinder. A likely reason for the formation of this second transition zone is the weight of the cylinder, which led to a compressive force approximately 55 N greater in the second transition zone than in the top transition zone.

As for the previous tests, during this test no new triangles folded while the force was rising, but many triangles folded in quick succession as the force dropped.

When fully folded, the cylinder had a height of 242 mm, compared with an original height of 872 mm. 150 mm of the compressed height was accounted for by the part of the cylinder fixed open at the base.

When the test was reversed, and the top plate moved up, the cylinder showed some spring-back, and regained a height of 540 mm. Closer inspection of the Cu-Be hinges, showed that the creases around the nodes had moved closer together by 1-2 mm. Stretching the cylinder caused these creases to move back towards their original position, and the cylinder to regain an extended configuration. The creases did not, however, return completely to their original position, and the cylinder only regained a height of 763 mm.

Three further tests were performed on this cylinder. After each test the cylinder was pulled back towards its original configuration. The force required to fold the cylinder in each case is plotted in Fig. 3(*b*). In each test the cylinder folded by forming a transition zone close to the base of the cylinder, which then moved up through the cylinder as the test proceeded. The force plotted is that in the transition zone, and so the original data has been modified to account for the steadily decreasing weight of the portion of the cylinder above the transition zone. Again during the test a number of triangles would fold each time the force decreased.

For each of the further three tests performed the change in the relative height coordinates of two successive nodes between the extended and folded configuration is 7 mm along the *a*-helix, and 45 mm on the *b*-helix. Note that these values are smaller than for the original test, as the plastic deformation around the nodes has reduced the height of the cylinder. Again, the basic periodicity of these force plots has a wavelength corresponding to relative height of successive nodes on the *b*-helix.

3 Discussion of Experiments

All the cylinders tested initially formed a transition zone, which then moved through the cylinder. Generally the zone moved from the top down, but for the Cu-Be and steel cylinder it moved from the bottom up, due to the self-weight of the cylinder. The shapes of the corresponding force plots also have a number of similarities. They all show a periodic variation of the force. In two of the cylinders, the Cu-Be and steel cylinder, and the Irathane and Al-alloy cylinder no. 1, the wavelength of this variation corresponds to the folding of successive nodes along the *b*-helix, i.e., of n pairs of triangles on the *a*-helix. In the Irathane and Al-alloy cylinder no. 2 the period of variation shows no obvious pattern.

Comparing these results with the computer simulation in Part II, a number of similarities can be seen. In both the simulation and the tests the modes of deformation of the cylinder are similar. A transition zone forms, which then moves through the cylinder. Comparing the plots of force from the computations with the experimental results, both cases show the force varying around a constant value as the transition zone moves through the cylinder.

There are, however, also a number of discrepancies. One is that the force in the experimental results does not vary about zero, but about an average compressive force. This implies that some strain energy is being stored in the cylinder during the folding process. Another discrepancy is that the actual force variation does not correspond to the height difference between successive nodes on the *a*-helix. Indeed, for two of the cylinders tested it corresponded to the height difference between successive nodes on the *b*-helix. A third discrepancy is the absence in the experimental results of any sign of an initial force peak, as the transition zone forms.

There is a fairly obvious explanation for the first discrepancy. The computer model in Part II assumed momentless hinges between the triangles. With this model, stretching energy builds up in the transition zone, at the start of the folding process and—once a certain energy level has been reached—the transition zone moves along the cylinder while the energy stored in the system remains constant. There is no bending energy anywhere in the cylinder. In reality, some energy must be put into the hinges to cause them to fold. Thus, as the transition zone moves down the cylinder, energy must be put into the cylinder to fold more hinges, and so the average compressive force must be greater than zero. It will be seen later that the effect of hinge stiffness explains the third discrepancy, the absence of an initial force peak.

To explain the second discrepancy, it should be noted that the most critical part of the manufacturing technique described in the Section 2 is the final joining process between the two edges of the sheet containing all the triangles. It is difficult to keep the two edges perfectly aligned during this process, and hence it is reasonable to expect that only one of the *b*-helices contains a series of geometric imperfections. Thus, if these imperfections are sufficiently large, the periodicity of the force plot would correspond to the folding of complete turns of the *a*-helix, not to the folding of successive pairs of triangles. The more random periodicity shown by the Irathane and Al-alloy cylinder no. 2 could be due to more distributed errors, as this was an early attempt at making a cylinder, and it had already been damaged by a number of demonstrations prior to the test.

4 Computer Modeling

In order to validate the reasons suggested in the previous section for the discrepancies between experimental results and those predicted by the computer simulation, two changes were made to the computer model described in Part II. The first change was to modify the model so that it no longer assumed momentless hinges between the triangles, and the second was to modify the model to simulate the effect of a final misalignment during the manufacture of a cylinder.

Elastic Hinges. The aim of this section is to describe how elastic hinges were incorporated into the computational model described in Part II. The original model was a pin-jointed truss, with bars of equal cross section along the edges of the triangles. This model was analyzed using the Force Method of structural analysis, and hence by setting up and solving appropriate systems of equilibrium and compatibility equations. To include in this model a series of elastic hinges that oppose relative rotations between adjacent triangles, the equilibrium, compatibility and flexibility matrices for a general hinge element are needed. In analogy with Section 2 of Part II, these matrices are derived directly in the global coordinate system. The stiffness matrix of a similar element was derived in Chapter 5 of Phaal (1990), using a transformation from a local coordinate system.

Consider a typical elastic hinge, Fig. 4, between two triangles. The triangle $\mathbf{P}_1\mathbf{P}_2\mathbf{P}_3$, Fig. 4($a$), has unit normal

$$\mathbf{u} = \frac{(\mathbf{P}_2 - \mathbf{P}_1) \times (\mathbf{P}_3 - \mathbf{P}_2)}{\|(\mathbf{P}_2 - \mathbf{P}_1) \times (\mathbf{P}_3 - \mathbf{P}_2)\|} \tag{1}$$

and triangle $\mathbf{P}_4\mathbf{P}_5\mathbf{P}_6$, Fig. 4($b$), has unit normal

$$\mathbf{v} = \frac{(\mathbf{P}_5 - \mathbf{P}_4) \times (\mathbf{P}_6 - \mathbf{P}_5)}{\|(\mathbf{P}_5 - \mathbf{P}_4) \times (\mathbf{P}_6 - \mathbf{P}_5)\|}. \tag{2}$$

Let M be the moment exerted by the hinge, positive in the direction shown in Fig. 4(a, b). Equilibrium of each triangle is maintained by three corner forces, normal to the triangle. Any in-plane force component exerts no in-plane moment, and hence makes no contribution to the equilibrium equations that are derived below. These in-plane forces are carried by the original truss model.

Consider the triangle $\mathbf{P}_1\mathbf{P}_2\mathbf{P}_3$, shown in Fig. 4($a$). The magnitude of the corner forces, r_1, r_2, r_3, can be found by considering moment equilibrium along the three sides of the triangle.

Taking moments initially about $\mathbf{P}_1\mathbf{P}_2$,

$$(\mathbf{P}_3 - \mathbf{P}_2) \times r_3\mathbf{u} \cdot \left(\frac{\mathbf{P}_2 - \mathbf{P}_1}{\|\mathbf{P}_2 - \mathbf{P}_1\|}\right) + M = 0, \tag{3}$$

rearranging the scalar triple product gives

$$\mathbf{u} \cdot (\mathbf{P}_2 - \mathbf{P}_1) \times (\mathbf{P}_3 - \mathbf{P}_2)\left(\frac{r_3}{\|\mathbf{P}_2 - \mathbf{P}_1\|}\right) + M = 0. \tag{4}$$

As $\mathbf{u}$ is a unit vector, and is parallel to $(\mathbf{P}_2 - \mathbf{P}_1) \times (\mathbf{P}_3 - \mathbf{P}_2)$, this can be written

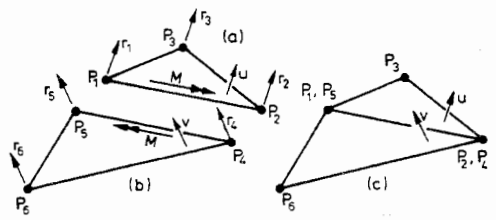

Fig. 4 Elastic hinge element

$$\|(\mathbf{P}_2 - \mathbf{P}_1) \times (\mathbf{P}_3 - \mathbf{P}_2)\|\left(\frac{r_3}{\|\mathbf{P}_2 - \mathbf{P}_1\|}\right) + M = 0 \tag{5}$$

and so

$$r_3 = -\frac{\|\mathbf{P}_2 - \mathbf{P}_1\|}{\|(\mathbf{P}_2 - \mathbf{P}_1) \times (\mathbf{P}_3 - \mathbf{P}_2\|)} M. \tag{6}$$

Similarly, taking moments about $\mathbf{P}_2\mathbf{P}_3$ gives

$$(\mathbf{P}_1 - \mathbf{P}_3) \times r_1\mathbf{u} \cdot \left(\frac{\mathbf{P}_3 - \mathbf{P}_2}{\|\mathbf{P}_3 - \mathbf{P}_2\|}\right) + \left(\frac{\mathbf{P}_2 - \mathbf{P}_1}{\|\mathbf{P}_2 - \mathbf{P}_1\|}\right) \cdot \left(\frac{\mathbf{P}_3 - \mathbf{P}_2}{\|\mathbf{P}_3 - \mathbf{P}_2\|}\right) M = 0 \tag{7}$$

which can be reduced to

$$r_1 = -\frac{(\mathbf{P}_2 - \mathbf{P}_1) \cdot (\mathbf{P}_3 - \mathbf{P}_2)}{\|(\mathbf{P}_3 - \mathbf{P}_2) \times (\mathbf{P}_1 - \mathbf{P}_3)\| \, \|(\mathbf{P}_2 - \mathbf{P}_1)\|} M. \tag{8}$$

Also, taking moments about $\mathbf{P}_3\mathbf{P}_1$ gives

$$(\mathbf{P}_2 - \mathbf{P}_1) \times r_2\mathbf{u} \cdot \left(\frac{\mathbf{P}_1 - \mathbf{P}_3}{\|\mathbf{P}_1 - \mathbf{P}_3\|}\right) + \left(\frac{\mathbf{P}_2 - \mathbf{P}_1}{\|\mathbf{P}_2 - \mathbf{P}_1\|}\right) \cdot \left(\frac{\mathbf{P}_1 - \mathbf{P}_3}{\|\mathbf{P}_1 - \mathbf{P}_3\|}\right) M = 0 \tag{9}$$

which can be reduced to

$$r_2 = -\frac{(\mathbf{P}_2 - \mathbf{P}_1) \cdot (\mathbf{P}_1 - \mathbf{P}_3)}{\|(\mathbf{P}_1 - \mathbf{P}_3) \times (\mathbf{P}_2 - \mathbf{P}_1)\| \, \|(\mathbf{P}_2 - \mathbf{P}_1)\|} M. \tag{10}$$

Similar relationships can be found for triangle $\mathbf{P}_4\mathbf{P}_5\mathbf{P}_6$

$$r_6 = -\frac{\|\mathbf{P}_5 - \mathbf{P}_4\|}{\|(\mathbf{P}_5 - \mathbf{P}_4) \times (\mathbf{P}_6 - \mathbf{P}_5\|)} M \tag{11}$$

$$r_4 = -\frac{(\mathbf{P}_5 - \mathbf{P}_4) \cdot (\mathbf{P}_6 - \mathbf{P}_5)}{\|(\mathbf{P}_6 - \mathbf{P}_5) \times (\mathbf{P}_4 - \mathbf{P}_6)\| \, \|(\mathbf{P}_5 - \mathbf{P}_4)\|} M \tag{12}$$

$$r_5 = -\frac{(\mathbf{P}_5 - \mathbf{P}_4) \cdot (\mathbf{P}_4 - \mathbf{P}_6)}{\|(\mathbf{P}_4 - \mathbf{P}_6) \times (\mathbf{P}_5 - \mathbf{P}_4)\| \, \|(\mathbf{P}_5 - \mathbf{P}_4)\|} M. \tag{13}$$

The equilibrium matrix for the general hinge element of Fig. 4(c) relates the moment M to all of the external forces in equilibrium with it. At $\mathbf{P}_1 = \mathbf{P}_5$, the total force is $r_1\mathbf{u} + r_5\mathbf{v}$, and similarly, at $\mathbf{P}_2 = \mathbf{P}_4$, the total force is $r_2\mathbf{u} + r_4\mathbf{v}$. At $\mathbf{P}_3$ and $\mathbf{P}_6$ the total forces are $r_3\mathbf{u}$ and $r_6\mathbf{v}$, respectively. Hence the 16×1 equilibrium matrix, $\mathbf{A}_h$, for this element is defined by the following system of equilibrium equations. For brevity, the notation $\mathbf{P}_{ij} = \mathbf{P}_j - \mathbf{P}_i$ has been adopted.

$$\begin{bmatrix} -\left(\frac{\mathbf{P}_{12} \cdot \mathbf{P}_{23}}{\|\mathbf{P}_{23} \times \mathbf{P}_{31}\| \, \|\mathbf{P}_{12}\|}\right)\mathbf{u} - \left(\frac{\mathbf{P}_{45} \cdot \mathbf{P}_{64}}{\|\mathbf{P}_{64} \times \mathbf{P}_{45}\| \, \|\mathbf{P}_{45}\|}\right)\mathbf{v} \\ -\left(\frac{\mathbf{P}_{12} \cdot \mathbf{P}_{31}}{\|\mathbf{P}_{31} \times \mathbf{P}_{12}\| \, \|\mathbf{P}_{12}\|}\right)\mathbf{u} - \left(\frac{\mathbf{P}_{45} \cdot \mathbf{P}_{56}}{\|\mathbf{P}_{56} \times \mathbf{P}_{64}\| \, \|\mathbf{P}_{45}\|}\right)\mathbf{v} \\ -\left(\frac{\|\mathbf{P}_{12}\|}{\|\mathbf{P}_{12} \times \mathbf{P}_{23}\|}\right)\mathbf{u} \\ -\left(\frac{\|\mathbf{P}_{45}\|}{\|\mathbf{P}_{45} \times \mathbf{P}_{56}\|}\right)\mathbf{v} \end{bmatrix} [M] = \begin{bmatrix} r_1\mathbf{u} + r_5\mathbf{v} \\ r_2\mathbf{u} + r_4\mathbf{v} \\ r_3\mathbf{u} \\ r_6\mathbf{v} \end{bmatrix} \tag{14}$$

The transpose of $\mathbf{A}_h$ is the compatibility matrix of the hinge element, relating the rotation of the hinge to the displacement of the nodes $\mathbf{P}_1 - \mathbf{P}_6$. It is assumed that the hinge element is unstrained; i.e., the hinge rotation is zero, when the element is flat, to simulate the behavior of a cylinder made from a flat sheet.

The flexibility matrix relates M to the hinge rotation. It is defined in terms of the axial flexibility of the bars in the truss model, the hinge length, and a dimensionless constant f, which can be varied to simulate different hinge properties. For the element of Fig. 4

$$\mathbf{F}_h = \left[\frac{f}{AE\,\|\mathbf{P}_2 - \mathbf{P}_1\|}\right]. \tag{15}$$

The hinge elements for the cylinder are incorporated into the truss model to give enlarged equilibrium, compatibility and flexibility matrices for the entire structure. For a cylinder with N nodes and B bars, there are now H hinge elements. Thus the vectors of generalized stresses and strains include, as well as all the terms defined in Part II, H additional components. Apart from these changes, the simulation algorithm is unchanged from Part II.

One of the cylinders analyzed in Part II has been reanalysed incorporating hinge elements along all internal bars. It has parameters $m = 1$, $n = 7$, $l_b/l_a = 1$ and $l_c/l_a = \sqrt{3}$. The particular model that has been analyzed has $N = 36$ nodes, $B = 86$ bars and $H = 76$ hinge elements. Each simulation of the folding process consists of approximately 300 compression steps of size $0.01l_a$. Simulations were performed using different values of the flexibility factor, f. The results for $f = 1 \times 10^6$, $f = 1 \times 10^5$ and $f = 1 \times 10^4$ are presented in Fig. 5. Note that decreasing f corresponds to making the hinges stiffer.

Figure 5(a) shows the force R required to compress the cylinder for the three different values of hinge stiffness. Each of the plots shows the force rising at the end, which is due to the interaction between the transition zone and the fully fixed base.

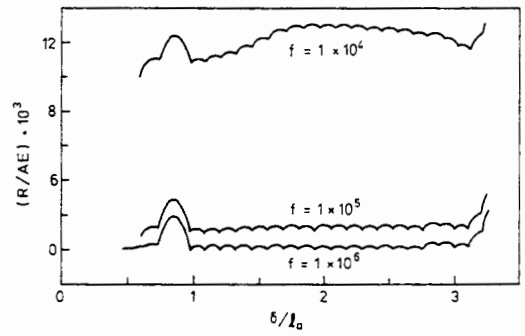

Fig. 5(a)

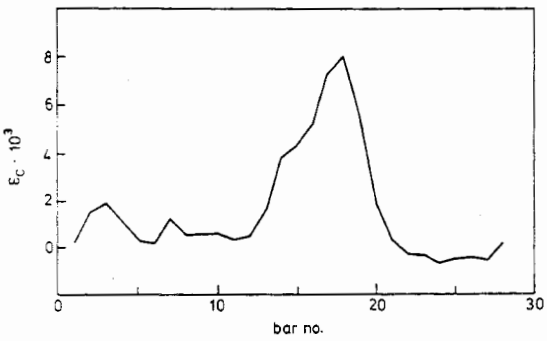

Fig. 5(b)

Fig. 5 Folding of cylinders with $m = 1$, $n = 7$, $l_b/l_a = 1$, $l_c/l_a = \sqrt{3}$: (a) force required to compress cylinders with different hinge flexibilities; (b) distribution of ϵ_c, when $\delta = 1.91l_a$ and $f = 1 \times 10^4$. Bars take the number of their bottom node, and nodes are numbered going up on the a-helix. Discrete values have been joined, for legibility.

When $f = 1 \times 10^6$ the force plot appears very similar to the results presented in Part II. The stiffness of the hinge has very little effect in this case.

When $f = 1 \times 10^5$ a larger peak force is required to form the transition zone at the top of the cylinder, and an approximately constant, nonzero force is required to move this zone down the cylinder.

When $f = 1 \times 10^4$, some clear changes in behaviour become evident, as the formation of the transition zone is now a two-stage process. During the first stage, the force R reaches a peak as the transition zone is initially formed at the top of the cylinder. This zone includes some bars which are also elastic hinges, and some which are not. The second stage occurs as this transition zone starts moving down the cylinder. R increases as the number of hinges in the transition zone increases. The transition zone is finally fully formed when *all* the bars within the zone are also elastic hinges. After this, there is a steady-state part of the plot as the fully formed transition zone moves down the cylinder. The steady-state part for this particular simulation is rather short, as the cylinder that is being simulated is small, and the effect of the base quickly becomes important. Note that there is an average compressive force in the cylinder during the steady-state phase, as energy must now be put into the cylinder to fold the hinges. Also note that the force required to form the initial transition zone is now seven times higher than for the case with momentless hinges. Finally note that the steady-state part of this plot involves compressive forces larger than those in the initial force peak.

Figure 5(b) shows the strain in the c-bars, defined in Fig. 2 of Part I when the cylinder has been compressed by $\delta = 1.91l_a$, for $f = 1 \times 10^4$. This value of δ corresponds to a peak in the force plot. The plots for $f = 1 \times 10^5$ and $f = 1 \times 10^6$ are similar, but with slightly lower strains. The plot is presented for $\delta = 1.91l_a$ rather than $\delta = 1.62l_a$, as used in Part 2, so that the transition zone has had time to fully form. The peak strain in the bars is only 2% higher when $f = 1 \times 10^4$ than for the case with momentless hinges.

Manufacturing Errors. The original computer model of the structure was also altered to assess the effect of misaligning the final seam of the cylinder during manufacture. These errors were simulated by imposing an initial strain e on the bars which cross the final join-line of the cylinder. Simulations were performed for cylinders with parameters $m = 1$, $n = 7$, $l_b/l_a = 1$ and $l_c/l_a = \sqrt{3}$ as before. The cylinders were compressed in approximately 300 steps of size $0.01l_a$ for three different values of e, 0.1 percent, 1 percent and 2.5 percent. The results are shown in Fig. 6.

When $e = 0.1$ percent, Fig. 6(a), the force plot is very similar to the case when the manufacturing error is zero.

When $e = 1$ percent, Fig. 6(b), however, the steady-state part of the plot becomes periodic with a wavelength corresponding to the folding of a set of $n =$ seven pairs of triangles, forming a complete turn of the a-helix. The manufacturing error prevents the folding from proceeding smoothly.

Similar results are obtained when $e = 2.5$ percent, Fig. 6(c). Again the results are periodic with a wavelength corresponding to the folding of $n =$ seven pairs of triangles. The variation in force is greater than for $e = 1$ percent as larger errors make it more difficult to fold parts of the cylinder.

Comparing the strain in the bars for the three cylinders containing manufacturing errors with a perfect cylinder, it is found that the peak strain is little changed. The largest increase occurs for $e = 2.5$ percent, when the peak strain is increased by 16 percent. However, because of the incompatibility introduced by making some bars longer, the manufacturing errors lead to generally higher levels of strain distributed throughout the cylinder.

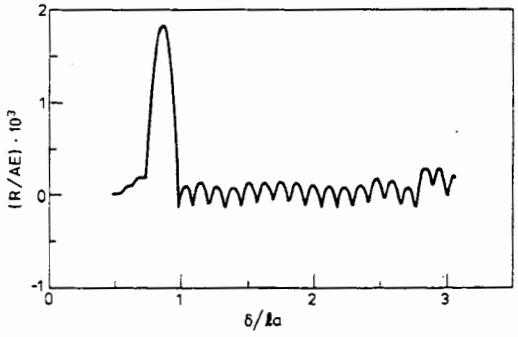

Fig. 6(a)

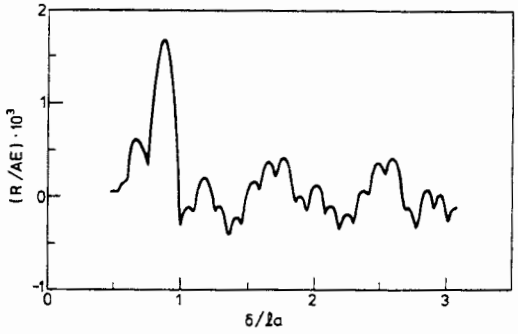

Fig. 6(b)

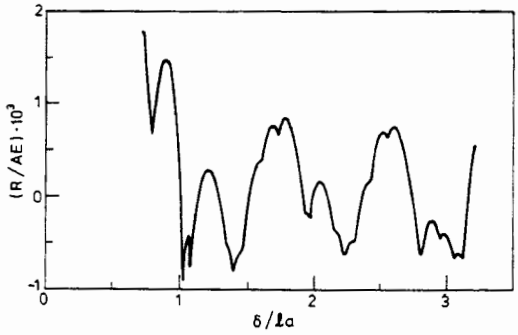

Fig. 6(c)

Fig. 6 Force required to compress initially strained cylinders with m = 1, n = 7, l_b/l_a = 1, $l_c/l_a = \sqrt{3}$: (a) e = 0.1 percent, (b) e = 1 percent, (c) e = 2.5 percent.

5 Discussion and Conclusions

This paper has shown the practical realization of the triangulated cylinders introduced in the previous two papers. In particular, it has explored two reasons why the experimental behaviour of these cylinders differs from the predictions obtained from the simple pin-jointed truss model analyzed in Part II.

The first effect that has been explored is the effect of hinge stiffness. It has been found that the effect of adding a series of elastic hinges to the truss model has the effect of raising the average compressive force to fold the models above zero, an effect seen in all of the cylinders tested. Indeed, sufficiently high hinge stiffnesses lead to the compressive force during steady-state folding being similar in size to the force required to form the initial transition zone. This explains why the initial force peak associated with the formation of the transition zone, predicted from the truss model in Part II, is not shown in the experimental results.

The second effect that has been explored is geometric misalignment during manufacturing. It has been found that the simple truss model predicts significant changes in behavior when geometric errors are introduced. The force developed, while still oscillating about zero, no longer has a period corresponding to the folding of one pair of triangles, but corresponds to the folding of n pairs of triangles. Superimposed on this global behavior is the folding of individual pairs of triangles. This behavior is very similar to that seen in the experimental tests.

Some consideration must be given to the values of the parameters used during the simulations. The initial strains e used to simulate manufacturing errors can be easily justified. The maximum value of e, 2.5 percent, corresponds to a misalignment during final fabrication of 3 mm for the Cu-Be and steel cylinder, and of 1 mm for the Irathane and Al-alloy cylinder. Errors of this magnitude could certainly have been introduced.

It is less easy to justify the particular values of f used during the investigation of the effects of hinge stiffness. The reason for this is the generic nature of the original model. In particular, the deformation of the bars in the original truss model was not meant to directly simulate the deformation of the triangular plates, but to investigate the effect of distributed elasticity within the model. In the Irathane and Al-alloy cylinders, for example, this deformation in fact takes place by shearing of the hinges. Thus as no quantitative measure of the bar stiffnesses has yet been considered, the values of f must be seen as a qualitative exploration of the effects of hinge elasticity on the folding process.

To validate the proposed computational model, a simulation of the behavior of the Irathane and Al-alloy cylinder no. 1 (see Table 1) has been performed. The simulation included both hinge elasticity and manufacturing errors, and the following parameters were chosen to match the observed behavior of the cylinder: $AE = 6 \cdot 10^5 N$, $f = 1.25 \cdot 10^7$, $e = 0.15$ percent. The initial behavior of the cylinder has not been simulated, because in the experimental model, extra, partially cut triangles were added at the top of the cylinder to form a level edge.

A comparison of the experimental results (reproduced from Fig. 1), and the simulation results, is shown in Fig. 7. The agreement between the results is remarkably accurate; both the periodicity, and the magnitudes of peaks and troughs, of the actual behavior are reproduced by the simulation.

Finally, it is interesting to note how this paper fits in with the work described in the previous two papers. The two Irathane and Al-alloy cylinders were of the simple type described in Section 1 of Part I made from isosceles triangles that fold down to prismatic stacks of plates. The Cu-Be and steel cylinder is not of this simple type, and was the first to be designed using the more general geometric formulation presented in the remainder of Part I to limit the amount of deformation required during folding.

The computational modelling techniques of Part II have been shown to predict many of the characteristics seen in the folding process. Also, although the changes to the model described here have radically changed some aspects of the compressive

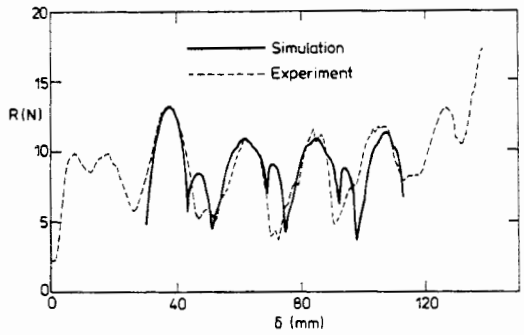

Fig. 7 Comparison of the force required to compress Irathane and Al-alloy cylinder no. 1, and a computer simulation

Table 2 Comparison of computational results for cylinders with $m = 1$, $n = 7$, $l_b/l_a = 1$, and $l_c/l_a = \sqrt{3}$

	$\lvert\epsilon_a\rvert_{max}$	$\lvert\epsilon_b\rvert_{max}$	$\lvert\epsilon_c\rvert_{max}$	R_{max}/AE
$1/f = 0$, $e = 0$	$5.0 \cdot 10^{-3}$	$6.9 \cdot 10^{-3}$	$8.7 \cdot 10^{-3}$	$1.8 \cdot 10^{-3}$
$1/f = 1 \cdot 10^{-4}$, $e = 0$	$4.8 \cdot 10^{-3}$	$7.8 \cdot 10^{-3}$	$8.9 \cdot 10^{-3}$	$13.1 \cdot 10^{-3}$
$1/f = 0$, $e = 2.5$ percent	$6.8 \cdot 10^{-3}$	$8.3 \cdot 10^{-3}$	$10.1 \cdot 10^{-3}$	$1.8 \cdot 10^{-3}$

behavior of the cylinder, the internal deformation of the cylinder during folding has not changed greatly. The maximum internal deformation, as measured by the strain in the c-bars of the model, has risen by no more than 16 percent in any simulation performed. A complete comparison of the computational results is made in Table 2. The original model remains a valid tool for predicting and comparing many aspects of the behavior of foldable cylinders, particularly the amount of deformation they undergo during folding. Also, the usefulness of having a simple computational model has been shown, as it can easily be modified to test the validity of different explanations for observed experimental behavior.

Acknowledgments

We would like to thank Mr. T. D. Wedgwood and Mr. K. Seffen for carrying out some of the experimental work described, and Mr. S. Vincer of Irathane International for supplying the Irathane coated plates. Financial support from British Aerospace (Space Systems) Ltd., and SERC is gratefully acknowledged.

References

Guest, S. D., and Pellegrino, S., 1994a, "The Folding of Triangulated Cylinders, Part I: Geometric Considerations," ASME JOURNAL OF APPLIED MECHANICS, Vol. 61, pp. 773–777.

Guest, S. D., and Pellegrino, S., 1994b, "The Folding of Triangulated Cylinders, Part II: The Folding Process," ASME JOURNAL OF APPLIED MECHANICS, Vol. 61, pp. 778–783.

Kyriakides, S., 1994, "Propagating Instabilities in Structures," *Advances in Applied Mechanics*, J. W. Hutchinson and T. W. Wu, eds., Academic Press, Boston, pp. 67–189.

Phaal, R., 1990, "A Two-Surface Computational Model for the Analysis of Thin Shell Structures," Ph.D. Dissertation, Cambridge University.